

Measuring Ambient Acidic Ultrafine Particles Using Iron Nanofilm Detectors: Method Development

Da-Wei Wang, Hai Guo & Chak K. Chan

To cite this article: Da-Wei Wang, Hai Guo & Chak K. Chan (2012) Measuring Ambient Acidic Ultrafine Particles Using Iron Nanofilm Detectors: Method Development, *Aerosol Science and Technology*, 46:5, 521-532, DOI: [10.1080/02786826.2011.643258](https://doi.org/10.1080/02786826.2011.643258)

To link to this article: <https://doi.org/10.1080/02786826.2011.643258>

 View supplementary material 

 Published online: 04 Jan 2012.

 Submit your article to this journal 

 Article views: 759

 View related articles 

 Citing articles: 1 View citing articles 



Measuring Ambient Acidic Ultrafine Particles Using Iron Nanofilm Detectors: Method Development

Da-Wei Wang,¹ Hai Guo,¹ and Chak K. Chan²

¹*Air Quality Studies, Department of Civil and Structural Engineering, The Hong Kong Polytechnic University, Hong Kong, China*

²*Division of Environment and Department of Chemical and Biomolecular Engineering, The Hong Kong University of Science and Technology, Hong Kong, China*

The number concentration and size-resolved properties of acidic ultrafine particles have been observed to more closely associate with adverse health effects than do indices of total particulate mass. However, no reliable measurement techniques are currently available to quantify the number concentration and the size distribution of ambient acidic ultrafine particles. In this study, a method with the use of iron nanofilm detectors for enumeration and size measurement of acid aerosols is developed and refined. Standard sulfuric acid (H₂SO₄) or ammonium hydrogen sulfate (NH₄H₂SO₄) droplets and sulfuric acid-coated particles were generated and deposited on the detectors causing reaction spots. The dimensions of the reaction spots were examined with Atomic Force Microscopy (AFM) to establish the correlations between the diameter of the particle and the size of the reaction spot. To validate this method, field measurements were conducted from September 06 to November 30, 2010, at Tai Mo Shan in Hong Kong. The results indicated that the particle number concentrations obtained from the AFM scanning of the exposed detectors via scanning mobility particle sizer (SMPS) and electrostatic precipitator (ESP) collection were comparable to those derived from the SMPS + CPC (condensation particle counter) measurements ($p > 0.05$). The average geometric mean diameter of particles at peak measured by the SMPS + CPC and the detectors scanned by the AFM was 52.3 ± 6.9 nm and 51.9 ± 3.1 nm, respectively, showing good agreement. It is suggested that the iron nanofilm detectors could be a reliable tool for the measurement and analysis of acidic particles in the atmosphere.

[Supplementary materials are available for this article. Go to the publisher's online edition of *Aerosol Science and Technology* to view the free supplementary files.]

Received 18 July 2011; accepted 6 November 2011.

This work is supported by the Environment and Conservation Fund (ECF) of the Hong Kong Special Administrative Region (ECF 20/2008).

Address correspondence to Hai Guo, Department of Civil and Structural Engineering, The Hong Kong Polytechnic University, No. 11, Yuk Choi Road, Hung Hom, Kowloon, Hong Kong, China. E-mail: ceguohai@polyu.edu.hk

1. INTRODUCTION

It is well documented that more than 90% of airborne particles in terms of number concentration are ultrafine particles (UFPs, particles with diameter less than $0.1 \mu\text{m}$) in both outdoor (USEPA 1996; Wichmann et al. 2000; Sioutas et al. 2005; Guo et al. 2008; Solomon et al. 2008; Zhu et al. 2008; Buonanno et al. 2009; Hagler et al. 2009) and indoor air (Abt et al. 2000; Wallace and Howard-Reed 2002; Wallace et al. 2008; Guo et al. 2010; Zhang and Zhu 2010; Wallace and Ott 2011). Due to their high diffusion coefficients and great accumulation ability in the regional lymph nodes and the lung, ultrafine particles can enter deep into the ciliated and alveolar sections of the lung (Morawska et al. 2004; Oberdörster et al. 2005; Bräuner et al. 2007; Stölzel et al. 2007) and even bloodstream (Schwartz 2001; Oberdörster et al. 2004), and contribute to negative health effects (Pope et al. 2002; Li et al. 2003; Diapouli et al. 2007; Andersen et al. 2010). As such, ambient UFPs may be more important than PM_{2.5} (particles with diameter less than $2.5 \mu\text{m}$) and PM₁₀ (particles with diameter less than $10 \mu\text{m}$) in terms of their number-associated (Diapouli et al. 2007; Hoek et al. 2008, 2010; Berghmans et al. 2009) and size-associated effects on human health (Ramgolam et al. 2008; Napierska et al. 2009; Sohaebuddin et al. 2010; Ulrich et al. 2011).

Although substantial toxicological evidence of the harmful effects of exposure to ultrafine particles exists, it is unlikely that all components of ultrafine particles are equally toxic (Utell et al. 1982; Schlesinger 1989; McGranahan and Murray 2003). Among all the chemical components, sulfuric acid (H₂SO₄) and ammonium bisulfate (NH₄H₂SO₄) are important chemicals in ultrafine particles in the atmosphere. In the last decade, a number of studies indicated the close association between the acidity of ultrafine particles and adverse health effects such as the prevalence of bronchitis symptoms and lung function decrements (Cohen et al. 2000, 2004b; Lippmann 2000; Thurston 2000; Wichmann et al. 2000b; Gwynn and Thurston 2001; Donaldson et al. 2002). Hence, understanding the levels of acidic ultrafine particles in the atmosphere is crucial for

epidemiologists to study the impact of ultrafine particles on human health.

Nevertheless, no reliable measurement techniques are available so far to obtain the number concentrations of acidic ultrafine particles due to the fact that determination of number concentration and size distribution of acidic ultrafine particles is an extremely difficult task. Thus, there is an urgent need to develop a method that can be used to quantify the number concentration of acidic ultrafine particles in the air.

As a matter of fact, some pilot studies were carried out to quantify the number of acidic particles. For instance, at the earliest study, Gerhard and Johnstone (1955) and Waller (1963) successfully obtained reaction spots of acidic particles in gelatinous films. However, it was impossible to individually detect droplets with diameter less than $1.0\ \mu\text{m}$ at that time. By measuring changes of light transmission and resistance of thin metal films, Lodge and Havlik (1960) used the changes as indicators of atmosphere pollution. Electronic micrographs of the exposed films showed extensive surface mottling and pitting of the metal films. Hayashi et al. (1961) used metal-coated glass slides to detect and size acid aerosols which were nebulized to form holes as reaction spots on the film surface, and also related the sizes of observed reaction pits to aerosol droplet diameters. Unfortunately, the smallest size of the acidic droplets that were characterized was several micrometers in diameter. Horstman et al. (1967) used thin iron-coated detectors, on which reaction pits were formed when the film was exposed to acidic particles, to size acidic particles with diameter much larger than $0.1\ \mu\text{m}$ by electron microscope. For submicrometer size particles, Bigg et al. (1974) developed a method of spot reaction by applying a thin film of reagent on the surface of the sample; later Mamane (1977) modified and improved this method specifically for soluble sulfates based on the reaction of the sulfate ion on barium chloride film. Huang and Turpin (1996) had also noted the ring formation as a characteristic of H_2SO_4 particles by scanning electron microscopy (SEM) on carbon film substrates. Most recently, Cohen et al. (2004a) developed iron nanofilm detectors by vapor deposition for the measurements of acidic particles in New York. The nanofilm detectors were examined with scanning probe microscopy (SPM) for the enumeration of reaction sites formed by acidic particles. In principle, this method could measure the size distribution and number concentration of ambient acidic ultrafine particles. However, no acidic particles were detected in their study, suggesting that the method might not be suitable for an atmosphere with low levels of air pollutants, or should be improved.

In Hong Kong, there have been few studies of the acidity of aerosols (Pathak et al. 2004; Yao et al. 2007). However, the aerosol acidity was characterized in terms of mass concentration, rather than number concentration. To the best of our knowledge, no study was conducted in Hong Kong to quantify the number concentrations of acidic ultrafine particles. Previous studies indicate that air pollution caused by particulate matter and ozone in the atmosphere of Hong Kong is serious (Pathak

et al. 2003, 2004; Wang et al. 2005; So et al. 2007; Yao et al. 2007; Guo et al. 2009). Hence, we chose Hong Kong as a proper location to test and improve the method of iron-film detectors so that reliable quantification of number concentration of acidic ultrafine particles can be obtained.

In order to obtain accurate number concentration of acidic ultrafine particles in the atmosphere of Hong Kong, this paper will mainly focus on the method development. The iron nanofilm coated on a silicon chip (i.e., the detector) used in previous study (Cohen et al. 2004b) was found to be easy to detach from the support under high humidity and high temperature. Hence, a variety of iron nanofilm detectors with more efficient and stable performance than those used in Cohen et al. (2004b) was developed in terms of substrate of the detectors and the coating methods. Standard acidic particles were generated and collected on the detectors. The sizes and shapes of reaction spots of generated acidic particles and the surface structure of the detectors were scanned by an Atomic Force Microscope (AFM), which was calibrated with known size polystyrene latex (PSL) particles, acidic droplets, and acid-coated carbon nanoparticles. Finally, the influence of temperature, relative humidity, and gaseous pollutants on the surface structure of the detectors was explored. A reliable method for the quantification of acidic ultrafine particles was established.

2. MATERIALS AND METHODS

2.1. Iron Nanofilm Detectors

Thermal Vacuum Evaporation (VE) and Magnetron Sputtering (MS) deposition are two methods commonly used for the coating of thin layer of ironfilm on the silicon wafer. In this study, about 25-nm-thick ironfilm was coated onto the silicon substrate by VE (Cooke Vacuum Products, USA) and by Direct Current (DC)-MS deposition of Fe (with purity of 99.999%) target (0.5 cm thick) in Ar (99.999%). The base pressure of the chamber was lower than 1×10^{-5} Pa before MS deposition and the total pressure for sputtering was kept at 1.0 Pa. Two types of substrates were used to support the ironfilms. The first substrate was silicon chips ($5\ \text{mm} \times 5\ \text{mm} \times 0.4\ \text{mm}$), which were ultrasonically cleaned in sulfuric acid solvent before coating. The second substrate was silicon chips ($5\ \text{mm} \times 5\ \text{mm} \times 0.4\ \text{mm}$) coated with a 5 nm titanium (Ti) layer by DC-MS system (ARC-12M, Plasma Science Inc., USA), for enhancing the adherence of the ironfilm on the substrates. Four batches of detectors, namely Fe-MS, Fe-VE, Fe-Ti-VE, and Fe-Ti-MS, were obtained and stored in a nitrogen atmosphere to avoid oxidation of the ironfilm surface except during exposure.

A control experiment was conducted to investigate the stability of the iron nanofilm surface of these four types of detectors under extreme weather conditions of high relative humidity (RH) and high temperature, and to study the adhesive strength of the iron nanofilm on the substrate with and without coating Ti layer. Blank detectors and a set of detectors that were previously

exposed to H_2SO_4 standard aerosols were placed in a container (desiccator) wrapped with a rubber belt heater to control temperature and RH for 3 months. The valve of the desiccator was open to ambient air. The RH and temperature were set to: i) 90% and 20°C; and ii) 85% and 35°C. These two weather conditions are often observed in subtropical Hong Kong.

To test whether gas-phase pollutants in the atmosphere affect the surface of the iron nanofilm detectors, a set of blank detectors were placed in a sealed plastic canister (height: 5 cm; diameter: 8 cm) with an inlet installed with a high-efficiency particle filter (HEPA) (Whatman, 0.3- μm pore size) to remove ambient particles. The diameter of the inlet and outlet was 0.5 cm. Particle-free air was pumped through the canister with a flow rate of 30 cm^3/min for the duration of the sampling period at a mountain site, i.e., Tai Mo Shan (TMS) (Section 2.4). The exposed detectors were scanned by AFM each week to check the impact of gaseous pollutants.

2.2. Standard Particle Generation and Collection

In order to obtain morphological information of acidic and nonacidic ultrafine particles on the designed iron nanofilm detectors and to calibrate the equipment such as SMPS + CPC, electrostatic precipitator (ESP) and AFM, both standard acidic and nonacidic particles were generated and collected onto the detectors in this study. Due to different physical and chemical properties of the standard acidic and nonacidic particles, the generation procedures of each were different while the collection procedures were the same. In this study, three different standard particles were separately generated and collected onto the designed iron nanofilm detectors. They were acidic droplet standards, acid-coated standard particles, and nonacidic standard particles. In principle, the three generated particles were charge-neutralized, size-selected by differential mobility analyzer (DMA), and deposited onto the nanofilm detectors using an ESP. Due to significant diffusion loss of particles with size below 10 nm and diffusion broadening effect in the transfer function, it is important to understand the efficiency (or penetration rate) of the DMA for the accurate measurement of airborne particles. In this study, an experimental system determining the aerosol losses in the DMA was established. In addition, the collection efficiency (or sampling performance) of the ESP was evaluated using PSL standards. The ESP used in this study was a point-to-plane electrostatic precipitator. The singly charged aerosol, leaving a DMA, was guided by a duct into the ESP, where perpendicular to the aerosol flow, an electrode with a flat round plate (20 mm in diameter) was fixed downstream a distance of 150 mm to the inlet. The detector, i.e., silicon chip (5 mm \times 5 mm \times 0.4 mm) coated with iron nanofilm was mounted on the plate by double-size tapes to collect the particles. It is noteworthy that a DMA was used prior to the ESP. This is due to the fact that DMA can charge particles using a bipolar charger (neutralizer) with radioactive sources, i.e., Am241, and the charged particles are easier than uncharged

particles to migrate to and are collected on a plate with the opposite charge in the electrical field. Detailed description on the calibration of the SMPS + CPC and ESP was given in Supplemental Information (S.I.). Here, we provided the detailed generation and collection procedures of the three acidic and nonacidic particles.

In principle, ambient acidic sulfates mainly exist in two forms: acid dissolved in aqueous droplets and as a surface layer on solid particles, such as typical carbonaceous or fly ash particles (Ronald et al. 1983; Lippmann 1989; Radojević and Harrison 1992). The second type of aerosol is formed by adsorption of sulfuric acid onto particles with large surface to volume ratio (Zhang et al. 2008). Hence, these two forms of H_2SO_4 standard particles were generated in this study.

To generate the acidic droplet standards, an aerosol generator (Model 7.811, GRIMM, Germany) was used to produce submicrometer-sized acidic droplets. The aerosol production rate can be adjusted by the flows of the atomizer and the dryer (dilution air). In this study, purified air with a flow rate of 4.8 L/min was introduced into the atomizer to generate polydisperse aerosols. Dilution air was added into the system at the exit of the generator with a flow rate of 10 L/min. Six sulfuric acid solutions with different concentrations (in H_2SO_4 (w)/ H_2O (v)), i.e., 0.09, 0.045, 0.009, 0.0018, 0.00036, and 0.000072 g/cm^3 were prepared to condition the droplets. The H_2SO_4 droplets were generated from each solution using the aerosol generator. For each solution, three different sizes, i.e., 32.5, 75.4, and 124.5 nm of H_2SO_4 droplets were selected by an SMPS (Model 5.400, GRIMM, Germany) separately, and each size of H_2SO_4 droplets was collected onto three detectors using an ESP (Model 5.561, GRIMM, Germany) with a steady voltage of 5000 V, respectively. The sampling flow rate of the ESP (0.3 L/min) was controlled by a CPC (Model 5.400, GRIMM, Germany). In this study, the sizes of the generated acidic droplets represented the electrical mobility diameter (D_m) measured by the SMPS, which meant the diameter of a sphere with the same migration velocity in a constant electric field as the particle of interest (Flagan 2001).

For the generation and collection of the submicrometer sulfuric acid-coated standard particles, a schematic diagram of the experimental system is shown in Figure 1. The system consisted of a nanocarbon particles generator, an H_2SO_4 aerosol evaporation and condensation system, an SMPS, an ESP, and a CPC. First, a large quantity of glucose aerosols was generated from D(+) Glucose monohydrate (Farco chemical) solution (5 g/100 mL H_2O) by an ultrasonic nebulizer (Model No. 402A1, China), and were introduced into a quartz tube furnace which was heated to 700°C (Model No. F21130-33, Barnstead Thermolyne, U.S.A.). At high temperature, without sufficient oxygen supply for combustion, the glucose aerosols underwent thermal decomposition, and produced ultrafine carbon particles. These generated carbon particles were diluted by air immediately in two conical flasks and then at a flow rate of 0.5 L/min passed over the surface of highly pure H_2SO_4 (98% w/w) heated on a wire

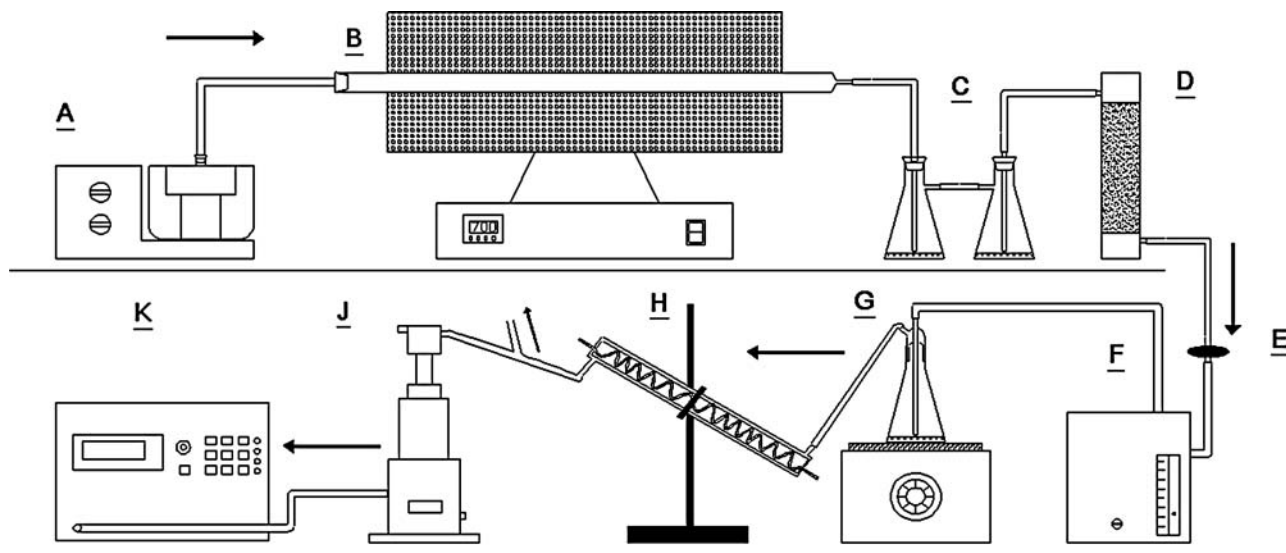


FIG. 1. The schematic of acid-coated nanoparticles generation and collection system. Note: **A** is the ultrasonic nebulizer; **B** is the quartz tube furnace; **C** are two conical flasks with purified water for cooling gas and removing large-size particles preliminarily; **D** is the silicone gel dryer to absorb the water mist; **E** is the filter to remove the particles with a size larger than $1\ \mu\text{m}$; **F** is a pump (0.5 L/min flow rate) to draw the carbon nanoparticles to **G**; **G** is the conical flask with highly pure H_2SO_4 for the generation of sulfuric acid vapor on a heater; **H** is the water-cooled condenser; **J** is SMPS + ESP; and **K** is CPC.

coil heater. The mixture of carbon particles and sulfuric acid vapor then passed through a thermostated water-cooled condenser to form nearly monodisperse sulfuric acid-coated aerosol. Ultimately, the generated acid-coated aerosol was classified by the SMPS and deposited onto the detectors mounted in the ESP with a flow rate of 0.3 L/min. Excess acid-coated aerosols (0.2 L/min) were absorbed by a H_2O solution through the bypass between the condenser and the SMPS. In this study, we used this H_2SO_4 coated aerosol generation system to produce six different sizes of acid-coated nanoparticles, namely 20.7, 32.5, 51.5, 75.4, 101.4, and 153.9 nm. The coated H_2SO_4 amount on particles was proportional to the exposure time, vapor concentration of H_2SO_4 , and particle surface area (or particle size) (Zhang et al. 2008). According to H_2SO_4 condensation results in this study and the results of Zhang et al. (2008), H_2SO_4 acid accounted for a fraction of 64.7%, 44.5%, 27.8%, 19.2%, 14.3%, and 9.5% of the mass of the six size particles, respectively. These different size acidic standards were collected on six detectors, respectively.

For the nonacidic particles, PSL microsphere standards (Duke Scientific Corp., USA) with physical diameters of 32, 46, and 102 nm were used for the generation and collection. One-two drops of PSL standard of each size were added into Milli-Q water to dilute the suspension and to minimize the concentration of impurities that may be present in tap water. The PSL aerosols, generated by an atomizer and diluted using filtered room air in a 1.5 liter bottle, were dried by a silica gel dryer (40 cm long \times 5 cm diameter), and then were introduced into the SMPS + CPC system. The singly charged aerosol, leaving from the bottom of the SMPS, was

then guided directly onto the nanofilm detectors mounted in the ESP.

2.3. Aerosol Analysis

In this study, the tapping mode of an AFM (NanoScope, Version 5.31R1, Veeco Instrument Inc., USA) was used to scan the acidic ultrafine particles or droplets collected on the iron nanofilm detectors. In the initial stage of this study, the AFM and a field emission scanning electron microscopy (FESEM) (JEOL-JSM 6335F, JEOL Ltd., Japan) were compared to verify that the AFM is more suitable and effective for the detection of acidic ultrafine aerosols. For detailed information about the methods and results, please refer to S.I.

The PSL microsphere standards, acidic droplet standards, and acid-coated standard particles generated in Section 2.2. were used to calibrate the AFM. In this study, the tapping mode of the AFM was used with a 5778E scanner. The oscillating probe tip in sharp pyramidal shape (ACT Series Probe) was used with a height of 14–16 μm and the nominal radius of curvature less than 10 nm. Scan parameters were established based on scan area and the imaging resolution of particles on the detectors. The $5\ \mu\text{m} \times 5\ \mu\text{m}$ areas on a detector at 512 sample line were selected for scanning with the parameters set as follows: scan rate: 0.6–0.8 Hz; amplitude setpoint: 0.65–0.80 V; integral gain: 0.2; and proportional gain: 0.5. With the use of these scan parameters, AFM was calibrated with known size PSL particles to define the AFM x , y , z -axis measurement accuracy which was mainly influenced by convolution of the pyramidal tip or the scanner sensitivity (see S.I. 3. Scanning of PSL microsphere standards), while laboratory-generated acidic droplets

and acid-coated carbon nanoparticles were used to confirm the correlation between measured dimensions of reaction sites and originally generated particle mobility diameter (D_m) sized by the SMPS.

2.4. Field Measurement

To assess the reliability and efficiency of the detectors, and to quantify the number concentrations of acidic ultrafine particles in the atmosphere of Hong Kong, a field measurement was conducted at Tai Mo Shan (TMS) from September 06 to November 30, 2010. TMS is the highest mountain (957 m a.s.l.) in Hong Kong urban area, dominating the central New Territories, north of Kowloon. Our sampling site was located near the mountain summit ($22^{\circ}24'38''$ N, $114^{\circ}07'28''$ E, about 700 m a.s.l.). In this field measurement, two sampling systems were utilized to characterize the ambient particles in the atmosphere. One was the SMPS + CPC used to measure the time-integrated size-resolved number concentration of ambient particles with a range of 5.5–350 nm at 4-min scan intervals. Another one was the SMPS + ESP used to collect particles smaller than 350 nm on iron nanofilm detectors. Due to high diffusion losses of particles with diameter less than 10 nm, 1 m flexible and conductive tubing was used in these two sampling systems. In the SMPS + ESP system, ambient particles were classified by SMPS and collected on a set of four detectors by ESP for 7 h each time with a flow rate of 0.3 L/min at the sampling site. The detector surface was then topographically analyzed by AFM to enumerate the acidic particles and size the acidic reaction spots. Consequently, by considering the penetration rate of the SMPS, the collection efficiency of the ESP, and the counting and sizing bias of the AFM, the number concentration and size distribution of acidic ultrafine particles in the ambient air at the sampling site were determined. Moreover, the total number concentration of particles calculated by the SMPS + ESP + AFM method

was compared with continuous data obtained from the SMPS + CPC system to further validate this method.

3. RESULTS AND DISCUSSION

3.1. Nanofilm Reaction Spots from Deposited Acidic Droplet and Acid-Coated Standards

Figure 2 shows the two-dimensional (2D) and three-dimensional (3D) images of a reaction spot caused by a 75.4 nm sulfuric acid droplet deposited on the 25-nm-thick iron nanofilm. This droplet was generated from the sulfuric acid solution of 0.009 g/cm³. The reaction site had a large bump due to the deformation of the iron film caused by the acidic droplet. The width of the reaction spot (horizontal distance 1-1, 2D image) on the detector was 310 ± 27 nm, about 4 times the diameter of the generated acidic droplet; and the vertical distance (0-1, 3D image) of the bump was 30.7 ± 5.3 nm, about two-fifths of the generated acidic droplet size.

Figure 3 presents the correlation between horizontal distance (width) of reaction spot scanned by AFM and the diameter of generated acidic droplets. The results showed that the width of the reaction spot of acidic droplets on the detectors was 2–4 times the diameter of generated particles (Figure 3, Ratio line). The width of the reaction spot was mainly dependent on the size of originally generated droplets and, to a lesser extent, the acidity. With the same acidity, the bigger the generated droplet, the larger the width of the reaction spot on the detector. It also clearly showed that the width of the reaction spot for large droplets (i.e., 75.4 and 124.5 nm) generated from H₂SO₄ solutions increased with the decrease in pH values of H₂SO₄ solutions, whereas the width for small droplet (i.e., 32.5 nm) remained constant.

The vertical distance (height) of the reaction spots also had an obvious increase with the increase in droplet size (Figure 4). In addition, with the increase of the acidity of H₂SO₄ solution,

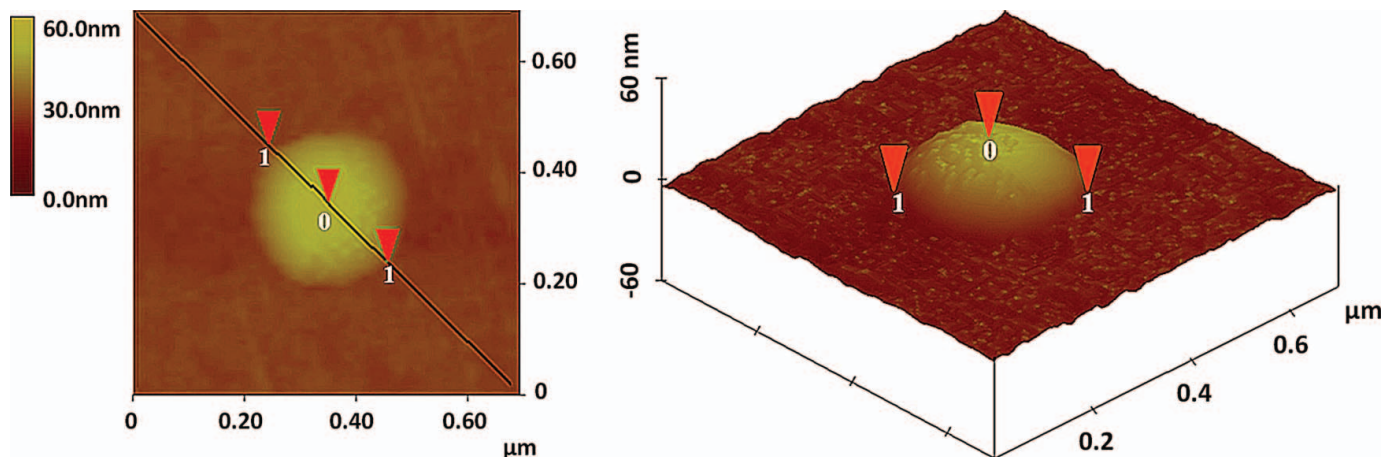


FIG. 2. Two-dimensional (2D) and three-dimensional (3D) images of a reaction spot caused by a 75.4 nm sulfuric acid droplet generated from the H₂SO₄ solution with a concentration of 0.009 g/cm³. (Color figure available online).

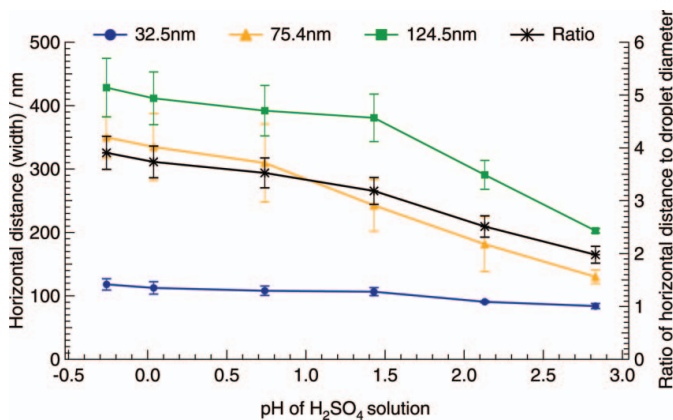


FIG. 3. Correlation between horizontal distance (width) of reaction spot scanned by AFM and the diameter of generated acidic droplets. The primary vertical axis represents the width of reaction spots; the secondary vertical axis represents the ratio of the width of reaction spots to the diameter of generated acidic droplets. The vertical error bars represent the deviation of the measurements. (Color figure available online).

the height of the reaction spot increased for each of the three size droplets, ranging from one-tenth to two-fifths, one-twentieth to two-fifths, and one-twenty-fifth to two-fifths of the size of the generated droplets, respectively. Moreover, the average ratio of the height of the reaction spot to the diameter of the corresponding droplet for the three size droplets obviously increased with the increase in acidity of H₂SO₄ solutions used to generate acidic droplets. It is noteworthy that at the same acidity, the ratio of the measured height to the diameter of corresponding droplet for the three size droplets was close with a low deviation, suggesting that the height of the reaction spot had a close correlation with the size of the generated droplets.

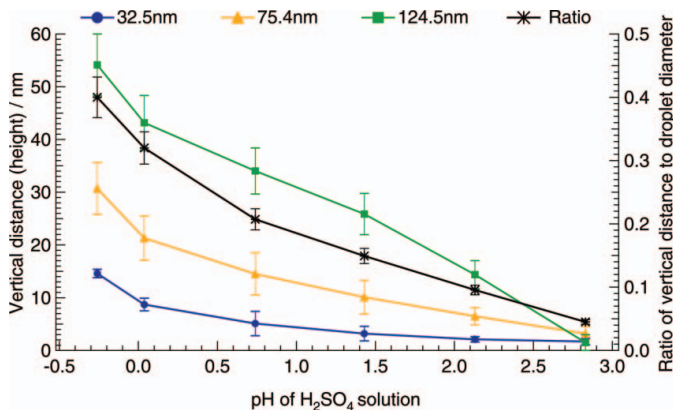


FIG. 4. Correlation between vertical distance (height) of reaction spot scanned by AFM and the diameter of generated acidic droplets. The primary vertical axis represents the height of reaction spots; the secondary vertical axis represents the ratio of the height of reaction spots to the diameter of generated acidic droplets. The vertical error bars represent the deviation of the measurements. (Color figure available online).

Figures 5a and b shows the 3D images of the reaction spots of a 32.5 nm and a 51.5 nm sulfuric acid-coated carbon particle on the iron nanofilm, respectively. The reaction site of the 32.5 nm sulfuric acid-coated particle had a large bump in the center surrounded by many extrusions (Figure 5a), whereas the reaction site of the 51.5 nm sulfuric acid-coated particle presented one large bump in the center surrounded by a circular ring (Figure 5b). The AFM-measured height and the width of the reaction spot for the 32.5 nm acidic particle were 11.8 nm and 108.2 nm, respectively, while for the 51.5 nm acid-coated particle, the height and width were 21.4 nm and 172.8 nm, respectively. The mechanism for such two different reaction spots was likely due to the fact that different surface to volume ratio of carbon particles caused different sulfuric acid adsorption onto particles, and subsequently different mass concentration of sulfuric acid on the surface of particles formed different morphology of reaction pits. To validate this assumption, we compared the differences of mass concentration between freshly generated carbon particles (before being exposed to H₂SO₄ vapor) and H₂SO₄ coated carbon particles in mobility size of 32.5 nm and 51.5 nm (after being exposed to H₂SO₄ vapor). The average mass ratio of 32.5 nm and 51.5 nm H₂SO₄ coated carbon particles to original carbon particles was 1.81 and 1.28, respectively, suggesting that a smaller size particle had a higher H₂SO₄ acid mass fraction, leading to a distinguished deformation on the surface of the iron nanofilm as shown in Figures 5a and b.

Good correlations were found between the dimension of the reaction spots and the mobility diameter of the generated acid-coated particles (Figure 6). That is, the width of the reaction spots formed on the 25-nm iron film detectors was approximately three times (3.2) the diameter of the corresponding acid-coated particles ($R^2 = 0.865$), and the height of the reaction spots was about one-third (0.32) the diameter of the corresponding acid-coated particles ($R^2 = 0.897$).

In previous studies, Horstman et al. (1967) found that measurements of the spot and acidic particle diameters by SEM yielded an average spot-to-particle diameter ratio of about 1.5 to 2. Cohen et al. (2000) illustrated that acid-coated carbon particles with a diameter of 100 nm produced clearly detectable reaction sites with the average height of 35 ± 16 nm (average \pm standard deviation) and the average width of 704 ± 230 nm, implying that the spot-to-particle diameter ratio was 5 to 9. In our study, the average height of the reaction spots for 100 nm acid-coated carbon particles was 28.3 ± 12 nm (about one-third of the particle diameter) and the average width was 316.4 ± 56 nm (approximately 3 times the particle diameter). The different spot-to-particle diameter ratios reported from different studies suggest that the dimension (width and height) of the reaction spot depends on the fraction of acid mass in the acid-coated particles, which could be different with the use of different acidic particle generation system, and on the characteristics of the iron nanofilm.

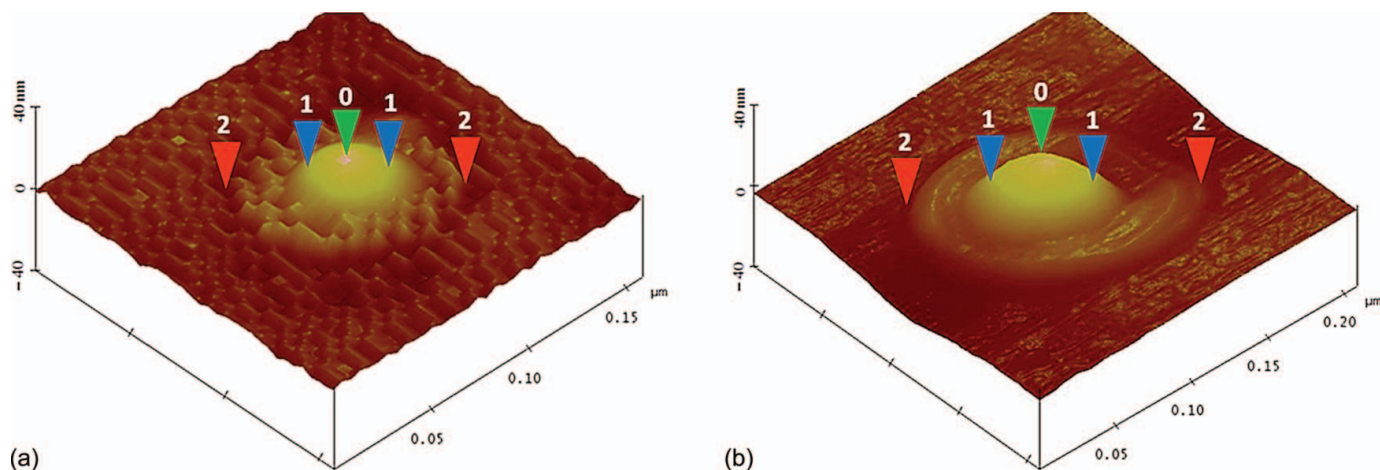


FIG. 5. Three-dimensional images of sulfuric acid-coated particle reaction spot on the 25-nm iron film; (a) A 32.5 nm acid-coated particle reaction spot; (b) A 51.5 nm sulfuric acid coated particle reaction spot. *Note:* The height of the reaction site above the iron-film surface was expressed as 0-2 vertical distance, and the width of the reaction site was taken as 2-2 horizontal distance i.e. maximum width of the reaction site. The central bump of the reaction site was taken as the width at half maximum value, shown as 1-1 horizontal distance. (Color figure available online).

3.2. Detector Response to Humidity, Temperature, and Gaseous Pollutants

During the 3-month exposure, the detectors were periodically examined visually and scanned with AFM. Visual observation of the exposed iron nanofilm detectors under the condition of 85% RH and 35°C showed that the surface of the Fe-VE and Fe-Ti-VE detectors with high number concentrations of standard acidic particles started to corrode after 2 weeks and was completely destroyed in 3 months. Compared to the AFM scan image before the exposure to high RH and temperature, the 32.5 nm sulfuric acid-coated carbon particles on the detectors under 85% RH and 35°C increased 2–3 times in diameter and 1.4–1.6 times in height. In contrast, the surfaces of the Fe-MS and Fe-Ti-MS detectors remained unchanged under the same weather condition for up to 3 months. Afterward, they were partly corroded. The results indicate that the Fe-MS and Fe-Ti-MS detectors had better stability than the Fe-VE and Fe-Ti-VE detectors, and the adhesive strength of iron film on the substrate with and without coating Ti layer had no obvious difference during the 3 months exposure in this study.

Under the condition of 90% RH and 20°C, the surface structure of the four types of detectors did not have significant changes after 3-month exposure, only the sizes of the reaction spots slightly increased during the exposure period. For instance, the Fe-Ti-MS detectors with acidic droplets exposed to 90% RH and 20°C for 3 months showed some enlargement of the reaction spots (Figures 7a and b). Figure 7a showed that the size of the reaction spots of 32.5 nm standard acid-coated particles on the detector was 112 ± 27 nm, 3–4 times the diameter of the standard particle. The height of the spot was 16 ± 8 nm, about one-half the diameter of the standard particle. After exposure to 90% RH and 20°C for 3 months, the dimension of the reaction site was enlarged horizontally and vertically to 162

± 43 nm and 20 ± 12 nm, respectively (Figure 7b). The results demonstrated that both RH and temperature influenced the surface feature of the detectors. High temperature with a high RH can significantly destroy the iron nanofilm. Furthermore, the results suggested that the Fe-MS and Fe-Ti-MS detectors were more resistant against extremely ambient conditions than the Fe-VE and Fe-Ti-VE detectors.

During the field measurement at TMS, Fe-VE nanofilm and Fe-MS nanofilm detectors were exposed to particle-free air to check if the ambient gases affected the surface of the detectors. The mean surface roughness of unexposed Fe-VE and Fe-MS nanofilm was 0.31 ± 0.17 nm and 0.28 ± 0.15 nm, respectively. The results of weekly quality control measurements on surface roughness showed that the average roughness in ten of $1 \mu\text{m}^2$ area on the blank Fe-VE and Fe-MS nanofilm detectors were 0.81 ± 0.44 nm and 0.64 ± 0.27 nm, respectively. Small

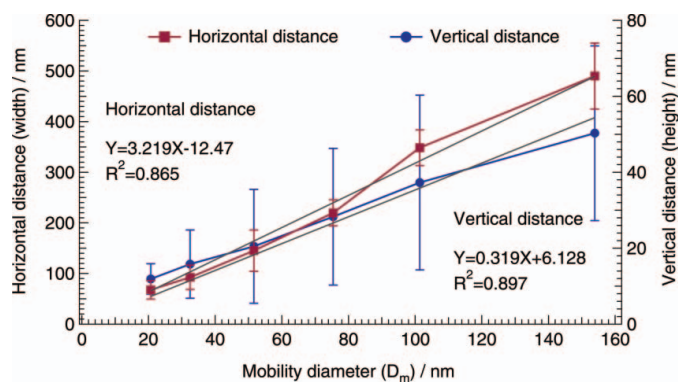


FIG. 6. Correlation between the dimension (width and height) of the reaction spots of acid-coated particles scanned by the AFM and the mobility diameter (D_m) of the acid-coated particles. The vertical error bars represent the deviation of the replicate measurements. (Color figure available online).

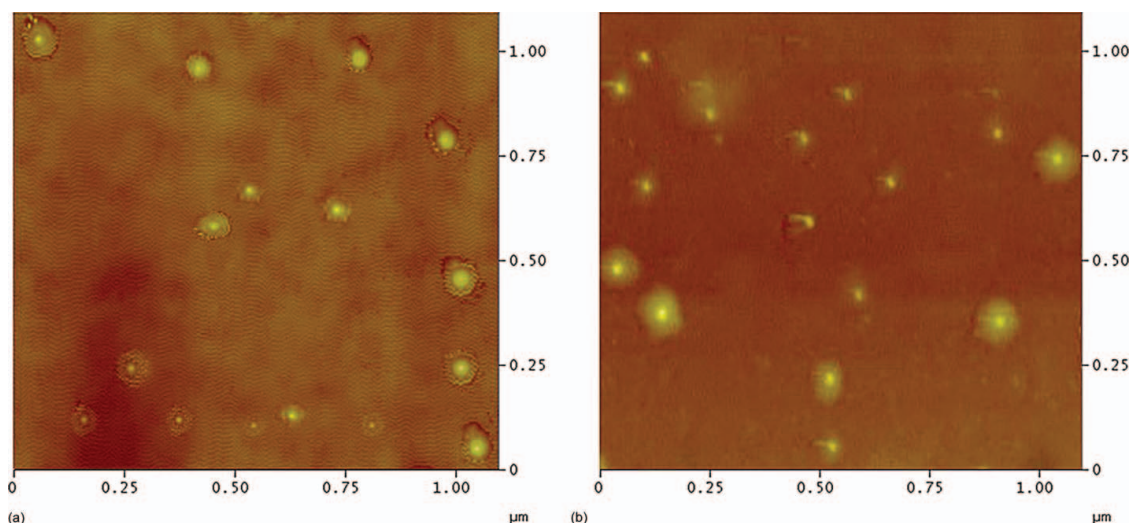


FIG. 7. AFM image of 32.5 nm acid-coated particles on Fe-Ti-MS detector; (a) AFM image before exposure to 90% RH and 20°C; (b) AFM image after 3-month exposure to 90% RH and 20°C. (Color figure available online).

standard deviation values demonstrated that the detector surface was very stable for both Fe-VE and Fe-MS nanofilm detectors, especially for Fe-MS detectors. Based on the variations of the surface roughness, the surface roughness of these blank detectors was about 3 times that of unexposed detectors for the sampling period, particularly in September and November, perhaps due to the interference of occasionally high humidity (range: 74.3%–99.8%) in September and/or high SO_2 (5.22 ppbv) and O_3 (67.41 ppbv) in November. Nevertheless, the increase in surface roughness had negligible effect on the quantification of acidic particles by AFM.

3.3. Validation in a Field Measurement

In the field measurement conducted at TMS, twenty-three groups of detectors (4 detectors per group, totally ninety-two detectors) were exposed to ambient air for 7 h and ultrafine particles were collected onto these detectors by an ESP on different sampling days at different time slots. According to the meteorological conditions and chemical composition of $\text{PM}_{2.5}$, i.e., high RH and high SO_4^{2-} , 16 detectors exposed on 22–25 November were preliminarily chosen for AFM scanning.

Figure 8a and b shows the AFM image of the exposed detectors collected during the sampling period. The acidic particles in the atmosphere deposited on the iron nanofilm detectors were easily distinguished from nonacidic particles (particles without surrounded rings and/or halos were assumed to represent nonacidic particles) in the atmosphere. Among a set of four detectors collected simultaneously, five of $100 \mu\text{m}^2$ areas of each detector were randomly selected to measure the sizes and to count the total number of nonacidic and acidic particles on these detectors by AFM, respectively. Thus, in total, twenty $100 \mu\text{m}^2$ scanning areas were obtained for each group of detector samples. Table 1 presents the sampling time slots and average

counts on each group of the detectors exposed in the sampling period (22–25 November 2010).

The AFM scanning results showed that the total number of nonacidic and acidic particles collected on the detectors was more than 200 counts per $100 \mu\text{m}^2$ scanning area. The size range of the nonacidic and acidic particles collected in field measurement was 7.5–386 nm and 7.4–312 nm, respectively. The diameter of nonacidic particles with peak value was larger than that of acidic particles, and both diameters with peak values changed on different sampling days. It is noteworthy that a remarkable number of acidic particles were below 20 nm, requiring high resolution scanning of $1 \mu\text{m} \times 1 \mu\text{m}$ areas to distinguish the acidic particles from nonacidic particles. Based on the number of nonacidic and acidic particles found on the detectors, the average number concentration of acidic particles in the atmosphere was estimated as follows.

In the field measurement conducted at TMS, the size range of nonacidic and acidic particles collected on the detectors on November 22, for example, was 8.5–375 nm and 7.5–248 nm, respectively. According to the setting of 44 channels in the SMPS, these measured nonacidic and acidic particles were categorized into 40 and 36 groups, respectively. The particle number concentration of each group was calibrated by the corresponding penetration rate of SMPS (PR_{SMPS} ; Figure S1) of these 44 channels, followed by the collection efficiency of ESP (E_{ESP}), of which, the size range was classified into four groups, i.e., <30 nm, 30–50 nm, 50–100 nm, and >100 nm. According to the known E_{ESP} values of the three size particles, i.e., 30, 50, and 100 nm, the E_{ESP} of particles with a size larger than 100 nm can be extrapolated from the correlation between the E_{ESP} and particle size. Thus, the E_{ESP} values for these four groups of particles were 74%, 80%, 86%, and 92%, respectively.

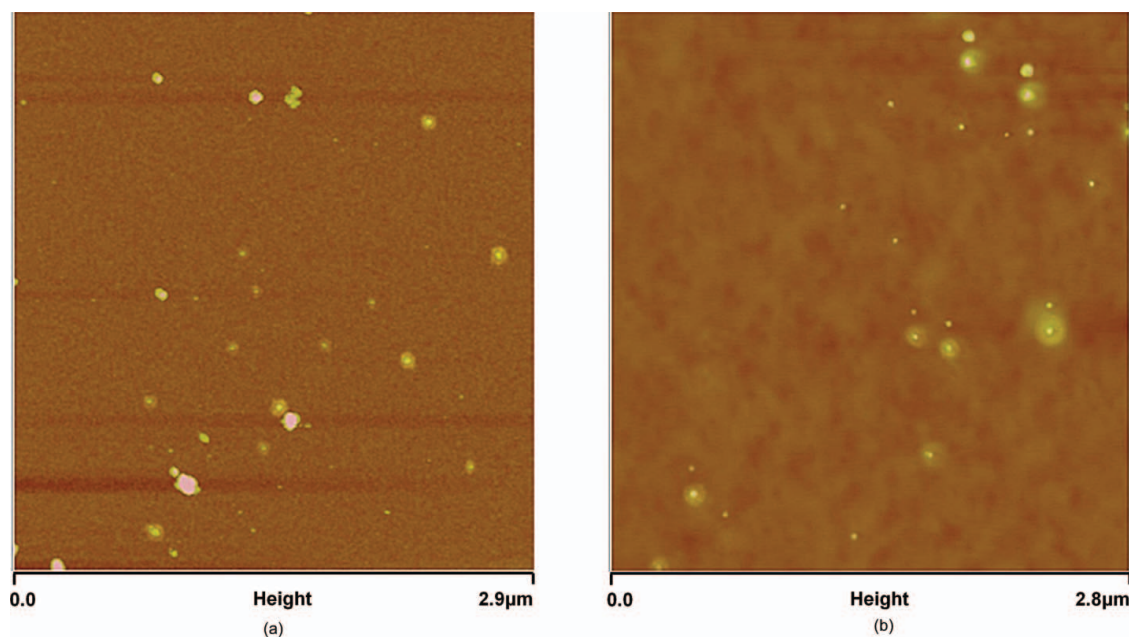


FIG. 8. Ambient acidic particles collected on the iron nanofilm detectors at TMS: (a) an AFM image with a $2.9 \mu\text{m} \times 2.9 \mu\text{m}$ scanning area on an Fe-MS nanofilm detector; (b) a $2.8 \mu\text{m} \times 2.8 \mu\text{m}$ scanning area on an Fe-VE nanofilm detector. (Color figure available online).

Since the collection plate of the ESP was a circle with a diameter of 20 mm, it had 3.14×10^6 $100 \mu\text{m}^2$ areas for AFM evaluation of the deposited particles. Hence, the ambient particles concentration, C_p , in particles per cm^3 , derived from the number of deposited particles, is given by $C_p = \Sigma 3.14 \times 10^6 N_i / (\text{PR}_{\text{SMPS } i} \times E_{\text{ESP } i} \times \text{Flow rate} \times \text{Time})$, where N_i is the total number of particles in i -size channel counted per $100 \mu\text{m}^2$; $\text{PR}_{\text{SMPS } i}$ is the penetration rate of the i -size channel particles; and $E_{\text{ESP } i}$ is the ESP collection efficiency of the i -size channel particles. The sampling flow rate was $300 \text{ cm}^3/\text{min}$. Since the

scanning time for each spectrum was 4 min and 5 s for each channel, the sampling time for each size channel was $7 \text{ h} \times 60 \text{ min/h} \times 5 \text{ s/4 min} = 525 \text{ s}$. By summing up the calculated number concentration of each size channel, the number concentration of the nonacidic and acidic particles on November 22 was $(4.60 \pm 0.86) \times 10^3/\text{cm}^3$ (peaked at $56.7 \pm 11.9 \text{ nm}$) and $(2.10 \pm 0.45) \times 10^3/\text{cm}^3$ (peaked at $47.7 \pm 8.4 \text{ nm}$), respectively. The total number concentration of ambient particles on November 22 was $(6.70 \pm 0.41) \times 10^3/\text{cm}^3$ (peaked at $51.6 \pm 10.8 \text{ nm}$). Similarly, the number concentrations of nonacidic and

TABLE 1
Acidic and nonacidic particles collected during the field measurement at TMS

Dates	Sampling time	Number of particles (mean \pm SD)		Size of particles (GMD \pm SD)*	
		Nonacidic particles per $100 \mu\text{m}^2$	Acidic particles per $100 \mu\text{m}^2$	Nonacidic particles size range and the diameter at peak per $100 \mu\text{m}^2$ (nm)	Acidic particles size range and the diameter at peak per $100 \mu\text{m}^2$ (nm)
22-Nov	15:00– 22:00	236.7 ± 85.3	64.3 ± 28.4	8.5–375 56.7 ± 11.9	7.5–248 47.7 ± 8.4
23-Nov	15:00– 22:00	147.2 ± 64.4	62.2 ± 32.5	9.4–386 62.8 ± 14.7	10.9–298 43.6 ± 18.4
24-Nov	15:00– 22:00	157.8 ± 68.5	58.2 ± 29.6	8.7–358 65.4 ± 21.8	7.4–312 50.4 ± 16.7
25-Nov	15:00– 22:00	194.6 ± 93.5	56.9 ± 32.4	7.5–316 49.6 ± 18.7	9.5–307 40.5 ± 11.2

*The size of nonacidic particles was verified using the results of AFM x and z calibrations; the diameter of acidic particle or acidic droplet was verified according to the ratios between the size of reaction spot and the acidic droplet or acidic particle (see Section 3.1).

TABLE 2

Comparison of the number concentration of ambient particles calculated by AFM with the values derived from the SMPS + CPC in the field measurement

Date	Sampling time	Number concentration of particles (mean \pm SD $10^3/\text{cm}^3$)			
		Nonacidic particles	Acidic particles	Total particles	SMPS + CPC data*
22-Nov	15:00–22:00	4.60 \pm 0.86	2.10 \pm 0.45	6.70 \pm 0.41	7.74 \pm 1.56
23-Nov		2.86 \pm 0.65	1.61 \pm 0.42	4.48 \pm 0.23	5.66 \pm 1.10
24-Nov		3.07 \pm 0.68	1.51 \pm 0.35	4.58 \pm 0.33	5.10 \pm 1.03
25-Nov		3.78 \pm 0.71	1.48 \pm 0.36	5.26 \pm 0.35	6.29 \pm 1.39

* For SMPS + CPC, the average hourly particle number concentration for the sampling period was calculated according to the trend of diurnal variation and the hourly averages for the nonsampling period. Two-tail *t*-tests between the ambient particle number concentration measured by the AFM and the SMPS + CPC at 15:00–22:00 on these four days indicated that the *p* value was larger than 0.05.

acidic particles and the total number concentration of ambient particles on the other three days (i.e. 23–25 November) were obtained (Table 2).

The total number concentration of particles calculated by the SMPS + ESP + AFM method was compared with continuous data obtained from the SMPS + CPC system. Due to the fact that only one SMPS was available for our study, the number concentration and size distribution of ambient particles measured by SMPS + CPC were not obtained at the same time as the sampling time of SMPS + ESP. According to the stable metrological conditions from November 20 to 29 and integrated SMPS + CPC data on November 20–21 and 26–29, the diurnal pattern of number concentration and size distribution was found to be similar on these days (data not shown here). Hence, it is reasonable to assume that the diurnal pattern of number concentration and size distribution on the sampling days of 22–25 November was the same as that on other days. Consequently, the mean number concentration and size distribution of particles between 15:00 and 22:00 of a day were derived from the data measured by the SMPS + CPC at other hours on the same day. The comparison of the total number concentrations counted on detectors with the values derived from the SMPS + CPC is shown in Table 2.

It was found that the total number concentrations of ambient particles measured by the ESP collection and AFM analysis of the detectors were well in line with the levels measured by the SMPS + CPC on these four days (two-tail *t*-test, *p* > 0.05). Moreover, the geometric mean diameter (GMD) of the particles at peak measured by these two methods showed remarkable agreement, namely, the average GMD at peak measured by the SMPS + CPC was 52.3 \pm 6.9 nm (45.8–60.3 nm) and the AFM measured average GMD at peak was 51.9 \pm 3.1 nm (49.1–56.3 nm). The results suggested that the iron nanofilm detectors could be a reliable tool for the measurement and analysis of acidic particles in the atmosphere, if more areas of the detectors were scanned and better resolution of the AFM images was achieved.

4. SUMMARY AND CONCLUSIONS

In this study, an iron nanofilm detector method was developed for the estimation of number concentration and size distribution of acidic particles in ambient air. Two new types of iron nanofilm detectors (i.e., Fe–Ti–MS and Fe–MS) were made and their surfaces and adhesion to silicon substrate remained stable when the surfaces of Fe–Ti–ED and Fe–ED detectors started to corrode after 2-week exposure under severe weather condition (85% RH and 35°C). However, under the condition of 90% RH and 20°C, the surface structure of the four types of detectors did not have significant changes at the end of the 3-month exposure period. Only some enlargement of the reaction sites was observed during the exposure period. In addition, ambient gases were found to have negligible effect on the surface roughness of the iron nanofilm detectors.

It is crucial to establish the relationship between reaction spots on the detector and the size of generated acidic droplets and acid-coated particles. To achieve the purposes, acidic droplets and acid-coated standard particles were generated. The results showed that for acidic droplets, larger droplet with the same acidity as smaller droplet had a larger horizontal distance (width) and vertical distance (height) of the reaction spot. The width of the reaction spot on the detectors was 2–4 times the mobility-based diameter of generated droplets. With the increase of the acidity of H₂SO₄ solution, the height of the reaction spot increased, ranging from one-twenty-fifth to two-fifths the mobility-based diameter of the generated droplets. For acid-coated particles, the width of reaction spots on the detectors was more than three times the mobility-based diameter of originally generated particle, while the height of reaction spots was about one-third of the original particle mobility diameter.

The developed iron nanofilm detectors were used in field measurement in order to prove that the method developed in this study was suitable for measuring the number concentration of acidic particles in the atmosphere. The number concentrations of ambient acidic particles, nonacidic particles, and total particles were measured using the detectors. The results

indicated that the total number concentrations of ultrafine particles measured on the iron nanofilm detectors were close to the number concentrations measured by the SMPS + CPC system ($p > 0.05$), and the average GMD of the particles at peak measured by AFM (51.9 ± 3.1 nm) had a good agreement with that measured by SMPS + CPC (52.3 ± 6.9 nm). Although the iron nanofilm detector method is time-consuming for AFM scanning, the field measurement results indicate that this method is promising and feasible for the detection and evaluation of the number concentration and size distribution of ambient acidic aerosols. To achieve a better performance of this method, it is important to possess an AFM with higher resolution.

REFERENCES

- Abt, E., Suh, H. H., Catalano, P., and Koutrakis, P. (2000). Relative Contribution of Outdoor and Indoor Particle Sources to Indoor Concentrations. *Environ. Sci. Technol.*, 34:3579–3587.
- Andersen, Z. J., Olsen, T. S., Andersen, K. K., Loft, S., Ketzler, M., and Raaschou-Nielsen, O. (2010). Association between Short-Term Exposure to Ultrafine Particles and Hospital Admissions for Stroke in Copenhagen, Denmark. *Eur. Heart J.*, 31:2034–2040.
- Berghmans, P., Bleux, N., Int Panis, L., Mishra, V. K., Torfs, R., and Van Poppel, M. (2009). Exposure Assessment of a Cyclist to PM₁₀ and Ultrafine Particles. *Sci. Total Environ.*, 407:1286–1298.
- Bigg, E. K., Ono, A., and Williams, A. J. (1974). Chemical Tests for Individual Submicron Aerosol Particles. *Atmos. Environ.*, 8:1–13.
- Bräuner, E. V., Forchhammer, L., Møller, P., Simonsen, J., Glasius, M., Wählin, P., et al. (2007). Exposure to Ultrafine Particles from Ambient Air and Oxidative Stress-Induced DNA Damage. *Environ. Health Perspect.*, 115:1177–1182.
- Buonanno, G., Ficco, G., and Stabile, L. (2009). Size Distribution and Number Concentration of Particles at the Stack of a Municipal Waste Incinerator. *Waste Manage.*, 29:749–755.
- Cohen, B. S., Li, W., Xiong, J. Q., and Lippmann, M. (2000). Detecting H⁺ in Ultrafine Ambient Aerosol Using Iron Nano-Film Detectors and Scanning Probe Microscopy. *Appl. Occup. Environ. Hyg.*, 15:80–89.
- Cohen, B. S., Heikkinen, M. S., Hazi, Y., Guo, H., Peters, P., and Lippmann, M. (2004b). Field Evaluation of Nanofilm Detectors for Measuring Acidic Particles in Indoor and Outdoor Air. *Res. Rep. Health Eff. Inst.*, Sep; (121, 1–35; discussion 37–46. PMID: 15553489 [PubMed – indexed for MEDLINE]
- Cohen, B. S., Heikkinen, M. S., and Hazi, Y. (2004a). Airborne Fine and Ultrafine Particles Near the World Trade Center Disaster Site. *Aerosol Sci. Technol.*, 38:338–348.
- Dixkens, J., and Fissan, H. (1999). Development of an Electrostatic Precipitator for Off-Line Particle Analysis. *Aerosol Sci. Technol.*, 30:438–453.
- Donaldson, K., Brown, D., Clouter, A., Duffin, R., MacNee, W., Renwick, L., et al. (2002). The Pulmonary Toxicology of Ultrafine Particles. *J. Aerosol Med.*, 15:213–220.
- Diapouli, E., Chaloulakou, A., and Spyrellis, N. (2007). Levels of Ultrafine Particles in Different Microenvironments—Implications to Children Exposure. *Sci. Total Environ.*, 388:128–136.
- Flagan, R. C. (2001). Electrical Techniques, in *Aerosol Measurement: Principles, Techniques, and Applications* (2nd ed.), P. A. Baron and K. Willeke, eds. John Wiley, New York, pp. 537–568.
- Gerhard, E. R., and Johnstone, H. F. (1955). Micro-Determination of Sulfuric Acid Aerosol. *Anal. Chem.*, 27:702–703.
- Guo, H., Ding, A. J., Morawska, L., He, C., Ayoko, G., Li, Y. S., et al. (2008). Size Distribution and New Particle Formation in Subtropical Eastern Australia. *Environ. Chem.*, 5:382–390.
- Guo, H., Ding, A. J., So, K. L., Ayoko, G., Li, Y. S., and Hung, W. T. (2009). and the Implication of Urban and Regional Contribution. *Atmos. Environ.*, 43:1159–1169.
- Guo, H., Morawska, L., He, C., Zhang, Y. L., Ayoko, G., and Cao, M. (2010). Characterization of Particle Number Concentrations and PM_{2.5} in a School: Influence of Outdoor Air Pollution on Indoor Air. *Environ. Sci. Pollut. Res.*, 17:1268–1278.
- Gwynn, R. C., and Thurston, G. D. (2001). The Burden of Air Pollution: Impacts among Racial Minorities. *Environ. Health Perspect.*, 109:501–506.
- Hayashi, H., Koshi, S., and Sakabe, H. (1961). Determination of Mist Size by Metal Coated Glass Slide. *Bull. NIIH*, 6:35–42.
- Hagler, G. S. W., Baldauf, R. W., Thoma, E. D., Long, T. R., Snow, R. F., Kinsey, J. S., et al. (2009). Ultrafine Particles Near a Major Roadway in Raleigh, North Carolina: Downwind Attenuation and Correlation with Traffic-Related Pollutants. *Atmos. Environ.*, 43:1229–1234.
- Horstman, S. W., Jr., Sanford, W., and Wagman, J. (1967). Size Analysis of Acid Aerosols by a Metal Film Technique. *Am. Ind. Hyg. Assoc. J.*, 28:523–530.
- Hoek, G., Kos, G., Harrison, R., de Hartog, J., Meliefste, K., ten Brink, H., et al. (2008). Indoor–Outdoor Relationships of Particle Number and Mass in Four European Cities. *Atmos. Environ.*, 42:156–169.
- Hoek, G., Boogaard, H., Knol, A., de Hartog, J., Slottje, P., and Ayres, J. G. (2010). Concentration Response Functions for Ultrafine Particles and All-Cause Mortality and Hospital Admissions: Results of a European Expert Panel Elicitation. *Environ. Sci. Technol.*, 44:476–482.
- Huang, P. F., and Turpin, B. (1996). Reduction of Sampling and Analytical Errors for Electron Microscopic Analysis of Atmospheric Aerosols. *Atmos. Environ.*, 30:4137–4148.
- Lodge, J. P., and Havlik, B. R. (1960). Evaporated Metal Films as Indicators of Atmospheric Pollution. *Int. J. Air Water Pollut.*, 3:249–252.
- Lippmann, M. (1989). Progress, Prospects, and Research Needs on the Health Effects of Acid Aerosols. *Environ Health Perspect.*, 79:203–205.
- Lippmann, M. (2000). *Environmental Toxicants: Human Exposures and Their Health Effects—Sulfur Oxides: Acidic Aerosols and SO₂*. John Wiley & Sons, New York, pp. 771–809.
- Li, N., Sioutas, C., Cho, A., Schmitz, D., Misra, C., Sempf, J., et al. (2003). Ultrafine Particulate Pollutants Induce Oxidative Stress and Mitochondrial Damage. *Environ. Health Perspect.*, 111:455–460.
- Mamane, Y. (1977). A Quantitative Method for the Detection of Individual Submicron Sulfate Particles. Ph.D. thesis, Pennsylvania State Univ., University Park, PA.
- Morawska, L., Moore, M. R., and Ristovski, Z. D. (2004). *Health Impacts of Ultrafine Particles*. Australian Department of the Environment and Heritage, Canberra, Australia.
- McGranahan, G., and Murray, F. (2003). *Air Pollution and Health in Rapidly Developing Countries*. Stockholm Environment Institute. Earthscan Publications Ltd., Oxford, UK, pp. 30–31.
- Napierska, D., Thomassen, L. C. J., Rabolli, V., Lison, D., Gonzalez, L., Kirsch-Volders, M., et al. (2009). Size-Dependent Cytotoxicity of Monodisperse Silica Nanoparticles in Human Endothelial Cells. *Small*, 5: 846–853.
- Oberdörster, G., Sharp, Z., Atudorei, V., Elder, A., Gelein, R., Kreyling, W., et al. (2004). Translocation of Inhaled Ultrafine Particles to the Brain. *Inhal. Toxicol.*, 16:437–445.
- Oberdörster, G., Oberdörster, E., and Oberdörster, J. (2005). Nanotoxicology: An Emerging Discipline Evolving from Studies of Ultrafine Particles. *Environ. Health Perspect.*, 113:823–839.
- Pathak, R. K., Yao, X. H., Alexis, K. H., and Chan, C. K. (2003). Acidity and Concentrations of Ionic Species of PM_{2.5} in Hong Kong. *Atmos. Environ.*, 37:1113–1124.
- Pathak, R. K., Louie, P. K. K., Chan, C. K. (2004). Characteristics of Aerosol Acidity in Hong Kong. *Atmos. Environ.*, 38:2965–2974.
- Pope, C. A., Burnett, R. T., Thun, M. J., Calle, E. E., Krewski, D., Ito, K., et al. (2002). Lung Cancer, Cardiopulmonary Mortality, and Long-Term Exposure to Fine Particulate Air Pollution. *J. Am. Med. Assoc.*, 287: 1132–1141.

- Radojević, M. and Harrison R. M. (1992). *Atmospheric Acidity: Sources, Consequences, and Abatement*. Environmental Management Series, Elsevier Science & Technology Publisher Ltd, Oxford, UK.
- Ramgolam, K., Chevaillier, S., Marano, F., Baeza-Squiban, A., and Martinon, L. (2008). Proinflammatory Effect of Fine and Ultrafine Particulate Matter Using Size-Resolved Urban Aerosols from Paris. *Chemosphere*, 72:1340–1346.
- Ronald, J. F., Allan, L. L., John W. W. (1983). Electron Microscopy of Acidic Aerosols Collected over the Northeastern United States. *Atmos. Environ.*, 8:1545–1561.
- Schlesinger, R. B. (1989). Factors Affecting the Response of Lung Clearance System to Acid: Aerosols Role of Exposure Concentration, Exposure Time, and Relative Acidity. *Environ. Health Perspect.*, 79:121–126.
- Schwartz, J. (2001). Air Pollution and Blood Markers of Cardiovascular Risk. *Environ. Health Perspect.*, 109 (Suppl. 3):405–409.
- Sioutas, C., Delfino, R. J., and Singh, M. (2005). Exposure Assessment for Atmospheric Ultrafine Particles (UFPs) and Implications in Epidemiological Research. *Environ. Health Perspect.*, 113:947–955.
- So, K. L., Guo, H., and Li, Y. S. (2007). Long-Term Variation of PM_{2.5} Levels and Composition at Rural, Urban, and Roadside Sites in Hong Kong: Increasing Impact of Regional Air Pollution. *Atmos. Environ.*, 41:9427–9434.
- Soderholm, S.C. (1979). Diffusion Measurements of Aerosols. Thesis [Ph.D.]—The University of Rochester, 1979. Source: Dissertation Abstracts International, Volume: 40–01, Section: B, p. 0304
- Solomon, P. A., Hopke, P. K., Froines, J., and Scheffe, R. (2008). Key Scientific Findings and Policy and Health-Relevant Insights from the U.S. Environmental Protection Agency's Particulate Matter Supersites Program and Related Studies: An Integration and Synthesis of Results. *J. Air Waste Manag. Assoc.*, 58:S-3–S-92.
- Sohaebuddin, S. K., Thevenot, P. T., Baker, D., Eaton, J. W., and Tang, L. (2010). Nanomaterial Cytotoxicity Is Composition, Size, and Cell Type Dependent. *Part. Fibre Toxicol.* 7:22.
- Stölzel, M., Breitner, S., Cyrus, J., Pitz, M., Wölke, G., Kreyling, W., et al. (2007). Daily Mortality and Particulate Matter in Different Size Classes in Erfurt, Germany. *J. Expo. Anal. Environ. Epidemiol.*, 17:458–467.
- Thurston, G.D. (2000). Particulate Matter and Sulfate: Evaluation of Current California Air Quality Standards with Respect to Protection of Children. Prepared for California Air Resources Board (CARB) and California Office of Environmental Health Hazard Assessment (OEHHA), Sacramento, CA. pp. 29–36.
- U. S. EPA. (1996). Air Quality for Particulate Matter, Vols. I, II, III, EPA/600/P-95/001aF, EPA/600/P-95/001bF, EPA/600/P-95/001cF.
- Ulrich, F., Olf, H., Stefan, R., Uwe, S., Michael, B., Ulrike, D., et al. (2011). Respiratory Effects of Indoor Particles in Young Children Are Size Dependent. *Sci. Total Environ.*, 409:1621–1631.
- Utell, M. J., Morrow, P. E., and Hyde, R. W. (1982). Comparison of Normal and Asthmatic Subjects Response to Sulphate Pollutant Aerosols. *Ann. Occup. Hyg.* 26:691–697.
- Waller, R. E. (1963). Acid Droplets in Town Air. *Int. J. Air Water Pollut.*, 7:773–778.
- Wallace, L. A., and Howard-Reed, C. (2002). Continuous Monitoring of Ultrafine, Fine, and Coarse Particles in a Residence for 18 Months in 1999–2000. *J. Air Waste Manag. Assoc.*, 52:828–844.
- Wallace, L. A., Wang, F., Howard-Reed, C., and Persily, A. (2008). Contribution of Gas and Electric Stoves to Residential Ultrafine Particle Concentrations between 2 and 64 nm: Size Distributions and Emission and Coagulation Rates. *Environ. Sci. Technol.*, 42:8641–8647.
- Wallace, L. A., and Ott, W. (2011). Personal Exposure to Ultrafine Particles. *J. Expo. Sci. Environ. Epidemiol.*, 21:20–30.
- Wang, T., Guo, H., Blake, D. R., Kwok, Y. H., Simpson, I. J., and Li, Y. S. (2005). Measurements of Trace Gases in the Inflow of South China Sea Background Air and Outflow of Regional Pollution at Tai O, Southern China. *J. Atmos. Chem.*, 52:295–317.
- Wichmann, H. E., Spix, C., Tuch, T., Wolke, G., Peters, A., Heinrich, J., et al. (2000). Daily Mortality and Fine and Ultrafine Particles in Erfurt, Germany. Part I: Role of Particle Number and Particle Mass. *HEI* 98: 5–86.
- Yang, K. M., Chung, J. Y., Hsieh, M. F., and Lin, D. S. (2007). Apparent Topographic Height Variations Measured by Noncontact Atomic Force Microscopy. *Jpn. J. Appl. Phys.*, 46:4395.
- Yao, X., Ling, T. Y., Fang, M., and Chan, C. K. (2007). Size Dependence of In Situ pH in Submicron Atmospheric Particles in Hong Kong. *Atmos. Environ.*, 41:382–393.
- Zhang, Q. F., and Zhu, Y. F. (2010). Measurements of Ultrafine Particles and Other Vehicular Pollutants Inside School Buses in South Texas. *Atmos. Environ.*, 44:253–261.
- Zhang, R. Y., Alexei, F. K., Joakim, P., Zhang, D., Xue, H. X., and McMurry, P. H. (2008). Variability in Morphology, Hygroscopicity, and Optical Properties of Soot Aerosols During Atmospheric Processing. *Proc. Natl. Acad. Sci. USA.*, 30:10291–10296.
- Zhu, Y., Fung, D. C., Kennedy, N., Hinds, W. C., and Eiguren-Fernandez, A. (2008). Measurements of Ultrafine Particles and Other Vehicular Pollutants Inside a Mobile Exposure System on Los Angeles Freeways. *J. Air Waste Manag. Assoc.*, 58:424–434.